Spatial and Source Multiplication Effects on the Area Ratio Reactivity Determination Method in a Strongly Heterogeneous Subcritical System

C. Berglöf
Department of Reactor Physics, Royal Institute of Technology, Albonova University Centre, SE-106 91 Stockholm, Sweden
Tel: +46 55378204, Email: calle@neutron.kth.se

M. Fernández-Ordóñez, D. Villamarín, V. Bécares, E. M. González-Romero
Nuclear Innovation Group, CIEMAT, Avda. Complutense, Madrid, Spain

Victor Bournos, Ivan Serafimovich, Sergei Mazanik, Yurii Fokov
Joint Institute for Power and Nuclear Research, National Academy of Sciences, Minsk, Belarus

Correspomding author: Carl Berglöf
Total number of pages (excluding this): 32
Total number of tables: 3
Total number of figures: 10

Spatial and Source Multiplication Effects on the Area Ratio Reactivity Determination Method in a Strongly Heterogeneous Subcritical System

C. Berglöf
Department of Reactor Physics, Royal Institute of Technology, Stockholm, Sweden
Tel: +46 55378204, Email: calle@neutron.kth.se

M. Fernández-Ordóñez, D. Villamarín, V. Bécares, E. M. González-Romero
Nuclear Innovation Group, CIEMAT, Avda. Complutense, Madrid, Spain

Victor Bournos, Ivan Serafimovich, Sergei Mazanik, Yurii Fokov
Joint Institute for Power and Nuclear Research, National Academy of Sciences, Minsk, Belarus

Abstract – *The area ratio method of Sjöstrand is generally considered as one of the most reliable reactivity determination methods and is thus a major candidate for offline calibration purposes in future accelerator-driven systems for high-level waste incineration. In this work, the Sjöstrand area ratio method has been evaluated experimentally under thorough conditions in the strongly heterogeneous subcritical facility YALINA-Booster. Both strengths and weaknesses of the method have been identified. Most surprisingly, it has been found that the area ratio reactivity estimates may differ a factor of two depending on detector position. It is also shown that this strong spatial dependence can be explained based on a simple two-region point kinetics model and corrected by means of correction factors obtained through Monte Carlo simulations. A new Monte Carlo correction method is proposed that includes, at the same time, the spatial disturbance and the effective delayed neutron fraction. In that way, a value of the effective multiplication factor is obtained from the measured dollar reactivity without the need of calculating the effective delayed neutron fraction explicitly and, thereby, the delayed neutron transport is performed*

only once. Further, it has been found that the Sjöstrand area ratio method is not sensitive to perturbations of the source multiplication factor.

I. INTRODUCTION

This paper presents a set of experiments aiming at finding a reliable and accurate way of obtaining the subcriticality of an accelerator-driven system (ADS). Recent studies on the Sjöstrand area ratio method [1] have shown that the method is the most stable and accurate method for subcriticality determination in terms of spatial dependence [2,3]. Thus, the Sjöstrand area ratio method has been chosen for further studies in a more complex configuration. In these experiments, carried out at the zero-power coupled fast-thermal subcritical facility YALINA-Booster [5], the Sjöstrand area ratio method, previously investigated in for instance references [1-4,6-9], has been studied in an extreme environment as a thorough validation for future offline use in a full-scale ADS. An important aspect of an ADS to be taken into consideration is its possible variation in source multiplication and source importance during operation due to for instance burnup. Thus, it is preferred to use a reactivity measurement method insensitive to source multiplication variations. The high flexibility of the subcritical facility allowed studying two configurations having the same subcriticality but different source multiplication factors associated with different source importance. This was obtained by substituting highly enriched fuel in the centre of the core (close to the neutron source) by low enriched fuel at the core periphery. In this way the effective multiplication factor (k_{eff}) could be kept constant while altering the source multiplication factor (k_s). This was done with an effective multiplication constant of ~0.95. In addition, a deep subcritical configuration (~0.85) was investigated to identify possible problems when applying the methods during core loading.

II. THE AREA RATIO REACTIVITY DETERMINATION METHOD

After accumulating detector data from many source neutron pulses a pulsed neutron source (PNS) histogram is obtained. From such a PNS histogram, the reactivity of the system can be estimated based on the point kinetics approach, provided that enough data have been accumulated and the fundamental mode overwhelms possible higher eigenmodes. Using the area ratio method by Sjöstrand [1], the reactivity expressed in units of dollars ($) is obtained from the ratio of the areas under the pulse described by the flux caused by prompt neutrons only (A_p) and the flux caused by delayed neutrons only (A_d), as given in the following expression:

$$\rho_{\$} \equiv \frac{\rho}{\beta_{eff}} = -\frac{A_p}{A_d}. \qquad (1)$$

Since the area ratio method is based on the point kinetics model no spatial dependence is taken into account. However, in a strongly heterogeneous core such as YALINA-Booster a spatial dependence is expected. Moreover, it should be noted that according to Eq. (1) the area ratio reactivity is source independent. In this work, the source multiplication has been altered at constant reactivity to verify the source multiplication independency of the method.

III. EXPERIMENTAL SETUP: THE YALINA-BOOSTER

The YALINA-Booster is a subcritical fast-thermal core coupled to a neutron generator [5]. The neutron generator uses accelerated deuterons impinging on a 45 mm Ti-T or Ti-D target, located at the core center, to produce fusion neutrons. In the experiments presented here the Ti-T target was used, thus providing a quasi-isotropic neutron energy spectrum of 14.1 MeV. The neutron generator can be operated in both continuous and pulsed modes and

gives thereby the possibility to perform both PNS measurements and continuous source measurements. The maximum beam current in continuous mode is around 1.5 mA giving a maximum neutron yield of approximately 10^{11} neutrons per second. In the experiments presented in this work, the neutron generator was operating in pulsed mode with a pulse width of 5 μs.

The core, depicted in Fig. 1, consists of a central lead zone (booster), a polyethylene zone, a radial graphite reflector and a front and back biological shielding of borated polyethylene. The fast spectrum lead zone and the thermal spectrum polyethylene zone are separated by a so called thermal neutron filter, or valve zone, consisting of one layer of 108 pins with metallic natural uranium and one layer of 116 pins with boron carbide (B_4C), which are located in the outermost two rows of the fast zone. Hence, thermal neutrons diffusing from the thermal zone to the fast zone are likely to be absorbed either by the boron or the natural uranium. In this way, a coupling of mainly fast neutrons between the two zones is maintained.

The booster has two sub-zones, the inner and outer booster, with different fuel pin pitch. Both booster sub zones could be loaded with 36% enriched uranium oxide fuel. The thermal zone was loaded with uranium oxide with 10% enrichment.

Three B_4C-control rods (CR) can be inserted in the thermal zone and allow changing the reactivity of the system by about 0.5 $. Hence, the sensitivity of the two reactivity monitoring techniques can be tested.

There are seven axial experimental channels (EC1B-EC4B and EC5T-EC7T) in the core, two axial (EC8R, EC9R) and two radial experimental channels (EC10R, EC11R) in the reflector. In addition, there is one neutron flux monitoring channel in each corner of the core (MC1-4) and one reference point outside the reactor (not shown in the figure). The detector at the reference point, a ^{3}He-detector (0.5NHI/IK [10]), was used for normalization

of experimental data acquired during different campaigns with interruptions for other experiments in between that could possibly change the source characteristics regarding strength, composition and beam alignment.

In the booster zone and the reflector it was necessary to use fission chambers having a large fissile deposit in order to reach sufficiently high count rates. Therefore, ^{235}U-fission chambers of 500 mg fissile deposit (KNT-31) were used. In the thermal zone, these detectors could not fit due to the limited diameter of the experimental channels. However, the smaller 1 mg ^{235}U-fission chamber (KNT-5) gave sufficient count rate. The ^{3}He-detector could not be used in any of the core regions due to saturation when operating the pulsed D-T source.

In addition to the in-core detectors and the reference point detector a source monitor was located in the forward beam direction. The source monitor, consisting of a liquid scintillator (BC501A), was calibrated to detected only neutrons above the fission neutron spectrum [11]. All other neutrons and gammas were disregarded by using a constant fraction discriminator (CFD). To reduce the gamma background further, the scintillator was placed behind a thick concrete wall.

Three core loadings, described in Table I and Fig. 2, were investigated. The aim when choosing the different loadings was to have two configurations with the same k_{eff} but different k_s and one deep subcritical configuration. All configurations, except SC6 were studied with the control rods both inserted and withdrawn, thus giving in total five configurations.

A complete description of the core design and the fission chambers is given in ref [12].

EXPERIMENTAL RESULTS

III.A General results and spatial effects

Characteristic PNS histograms for the three core regions booster zone, thermal zone and reflector are shown in Fig. 3 for configuration SC3a. It should be stressed that the EC6T data have been acquired with a less efficient detector, thus yielding less counts per second. That is why the EC6T data is lower although the flux is expected to be the highest in the thermal zone.

The most interesting behavior can be found in the data from the fission chamber located in the booster region. There is a very fast flux decay within a few microseconds after the source pulse insertion. During this time, the flux decreases two orders of magnitude. This part of the histogram is shown in detail in Fig. 4 together with data from EC2B, EC3B, EC5T and the source monitor. From the figure it is possible to see that the shape of the flux peak follows the shape of the source until the source is switched off. Then a very fast decay follows, composed of two decay modes during 5-6 μs and 6-10 μs respectively. It may be assumed that the fastest mode ($-1.3 \cdot 10^6$ s^{-1}) is caused by the removal of source neutrons and the second one reflects a decay constant characteristic of the fast zone of about $-4.4 \cdot 10^5$ s^{-1}. After about 15 μs, neutrons from the thermal zone, of various energy regimes, start to dominate the total flux in the booster zone. In EC3B, a higher flux is noticed after about 10 μs. This is caused by a fast neutron flux rebound from the thermal zone; weakly affected by the valve zone. The signal from EC5T (in the inner part of the thermal zone) shows a clear similarity to EC3B, indicating a significant neutron leakage through the valve zone.

As can be seen in Fig. 4, the source has a tail reaching from 5 μs to about 11 μs. This tail stems primarily from scattered source neutrons and first generation fission neutrons and gammas reaching above the CFD threshold.

Returning to Fig. 3, a joint prompt neutron decay can be found in all detectors from about 1 ms (somewhat later in the reflector) to about 6 ms. During this decay, the flux is, in the entire core, driven by the fundamental mode of the thermal region. This means that despite the complex heterogeneity of the core there exists a global prompt neutron decay constant in the core.

The most important observation from these measurements is the large deviation in reactivity given by the Sjöstrand area ratio method obtained using the booster region detectors. As can be seen in Table II, the absolute value of the reactivity when measured in the booster region can be up to a factor of two larger than the corresponding measurement in the thermal region or the reflector. Obtaining a lower reactivity with the booster detectors is expected since the rest of the core is partly decoupled by the valve zone. Another contribution stems from the close location of the detector to the source, thus strengthening the effects of higher eigenmodes and making the prompt area non-representative to the core averaged prompt flux and violating the assumption that the fundamental mode must be dominating. The large peak found in the booster PNS histograms during the first 10 μs contributes strongly to the prompt area, in the worst case up to 40%. These neutrons are direct or scattered source neutrons and multiplied neutrons from fission and (n,xn)-reactions in lead. An indication of this contribution can be seen in Table II when comparing the area ratio reactivities in EC1B, EC2B and EC3B for SC3a (CR In) and SC3b (CR In and Out). As the distance to the source increases, the amplitude of the source mode decreases and the reactivity values approaches those of the thermal zone.

In the deep subcritical state (SC6), the same characteristic spatial spread of a factor of two is observed. There is no indication of deteriorated performance of the area ratio method at this reactivity level, although the prompt decay seems to be strongly biased in the reflector (Fig. 5).

Fig. 6 displays two PNS histograms from the same configuration and detector position. The only difference between the two histograms is the control rod position. As expected, the prompt decay is faster when having the control rods inserted, which can be observed by eye. The reactivity introduced by the control rods can be traced by the area ratio method, as can be found in Table II.

In the context of high-power system design, the heterogeneity of this experiment is extreme, but the results may have some implications on the instrumentation of a full-scale accelerator-driven system. If using burnable absorbers or having a high local content of nuclides with large absorption cross section, such as ^{241}Am, in a loosely coupled heterogeneous loading, it should be avoided to locate the detector close to the absorber or the source. Otherwise, the margin to criticality, when measured by the area ratio method, might locally be under-estimated. Burnable absorbers are not foreseen at least in one of the latest ADS designs [14], but having a large fraction of Am is a key feature.

III.B Source Multiplication Effects

The layout of configurations SC3a and SC3b was designed through MCNP simulations to give the same value of k_{eff} with as large perturbation of the inner booster zone as possible. The source multiplication, defined as

$$k_s = \frac{M}{M+S}, \tag{2}$$

where M is the total neutron production and S is the external source strength [15], was also estimated by MCNP calculations. It was found that the difference in k_s between SC3a and SC3b is approximately 500 pcm due to the variation of the source neutron importance. The purpose of the measurements on SC3a and SC3b was to identify a possible influence of k_s on the area ratio technique. It was found that there was a major difference in the shape of the PNS histograms during the first microseconds after the pulse insertion. This part of the PNS histogram is, for the booster region (EC1B and EC2B), shown in Fig. 7 for configurations SC3a and SC3b. The histograms are normalized to the reference detector count rate to correct for different source strengths. In the thermal zone, on the other hand, the two configurations provide very similar PNS histograms (Fig. 8). In Fig. 9, the reactivity difference between configurations SC3a and SC3b is plotted together with the introduced source reactivity change in units of dollars ($). When doing a comparison, one must keep in mind that it is assumed that a possible difference in effective delayed neutron fraction between the two configurations is negligible. As can be seen, despite the large difference in PNS histogram shape shown in Fig. 7, the area ratio reactivity estimates are comparable and not visibly affected by the source reactivity perturbation.

IV. TWO-REGION POINT KINETICS MODEL

The simplest way to describe the deviating results obtained by the Sjöstrand area ratio method in the fast booster zone is to extend the point kinetics equations to two regions. This has, for the Sjöstrand area ratio method, previously been done for a core-reflector system [4], but is here adopted for the fast-thermal part of the active core. By treating the flux caused by prompt neutrons, n_p, and delayed neutrons n_d, separately, an analytical solution to the area ratio reactivity, Eq. (1), can be obtained [16]. Following the procedure and notation described in references [16,17], a two-region point kinetics model with

prompt and delayed neutron fluxes and external source strength S can be expressed as follows:

$$\begin{cases} \dfrac{dn_{p1}(t)}{dt} = \alpha_1 n_{p1}(t) + \dfrac{f_{21}}{\tau_2} n_{p2}(t) + S(t) \\ \dfrac{dn_{d1}(t)}{dt} = \alpha_1 n_{d1}(t) + \dfrac{f_{21}}{\tau_2} n_{d2}(t) + \lambda C_1(t) \\ \dfrac{dC_1(t)}{dt} = \dfrac{\beta_1}{\Lambda_1}\left(n_{p1}(t) + n_{d1}(t)\right) - \lambda C_1(t) \\ \dfrac{dn_{p2}(t)}{dt} = \alpha_2 n_{p2}(t) + \dfrac{f_{12}}{\tau_1} n_{p1}(t) \\ \dfrac{dn_{d2}(t)}{dt} = \alpha_2 n_{d2}(t) + \dfrac{f_{12}}{\tau_1} n_{d1}(t) + \lambda C_2(t) \\ \dfrac{dC_2(t)}{dt} = \dfrac{\beta_2}{\Lambda_2}\left(n_{p2}(t) + n_{d2}(t)\right) - \lambda C_2(t) \end{cases} \quad (3)$$

In this set of equations n_{pi} is the prompt neutron flux density in region i, n_{di} is the delayed neutron flux density in region i, C_i is the delayed neutron precursor density in region i, α_i is the local prompt neutron decay constant in region i, f_{ij} is the probability that a neutron escapes from region i to region j, τ_i is the local neutron lifetime in region i, β_i is the local effective delayed neutron fraction in region i, Λ_i is the local mean neutron reproduction time in region i and λ is the one delayed neutron precursor group decay constant. In the case of YALINA-Booster, region 1 is the booster region, where the source is located, and region 2 is the thermal zone.

The neutron flux areas of Eq. (1) are obtained by integrating the neutron fluxes from zero to infinity. If assuming a Dirac source pulse, the left hand side of Eq. (3) will be zero:

$$\begin{cases} 0 = \alpha_1 A_{p1} + \dfrac{f_{21}}{\tau_2} A_{p2} + S_0 \\ 0 = \alpha_1 A_{d1} + \dfrac{f_{21}}{\tau_2} A_{d2} + \dfrac{\beta_1}{\Lambda_1}\left(A_{p1} + A_{d1}\right) \\ 0 = \alpha_2 A_{p2} + \dfrac{f_{12}}{\tau_1} A_{p1} \\ 0 = \alpha_2 A_{d2} + \dfrac{f_{12}}{\tau_1} A_{d1} + \dfrac{\beta_2}{\Lambda_2}\left(A_{p2} + A_{d2}\right) \end{cases} \quad (4)$$

Here, S_0 is the number of neutrons in the source pulse. An expression of the measured area ratio reactivity in each region can be derived by solving for the ratios of prompt and delayed areas in the two regions: A_{p1} / A_{d1} and A_{p2} / A_{d2}.

$$\rho_{\$1} = -\frac{A_{p1}}{A_{d1}} = \frac{(\alpha_1\Lambda_1 + \beta_1)(\alpha_2\Lambda_2 + \beta_2) - f\frac{\Lambda_1\Lambda_2}{\tau_1\tau_2}}{(\alpha_2\Lambda_2 + \beta_2)\beta_1 + f\frac{\Lambda_1}{\tau_1\tau_2\alpha_2}\beta_2} \tag{5}$$

$$\rho_{\$2} = -\frac{A_{p2}}{A_{d2}} = \frac{(\alpha_1\Lambda_1 + \beta_1)(\alpha_2\Lambda_2 + \beta_2) - f\frac{\Lambda_1\Lambda_2}{\tau_1\tau_2}}{(\alpha_1\Lambda_1 + \beta_1)(\alpha_2\Lambda_2 + \beta_2) - \alpha_1\Lambda_1\alpha_2\Lambda_2} \tag{6}$$

In these equations f is the return probability [17]:

$$f = f_{12} f_{21}. \tag{7}$$

By assuming

$$|\alpha_1| \ll |\alpha_2|, \tag{8}$$

which is true for YALINA-Booster, the global area ratio reactivities can be expressed as

$$\rho_{\$1} \approx \frac{\rho_2}{\beta_2}\left(\frac{1}{f}\alpha_1\tau_1\alpha_2\tau_2 - 1\right) + 1 \tag{9}$$

and

$$\rho_{\$2} \approx \frac{\rho_2}{\beta_2}\left(1 + f\frac{1}{\alpha_1\tau_1}\right) - f\frac{1}{\alpha_1\tau_1\beta_2}, \tag{10}$$

where ρ_2 is the local reactivity in region 2 obeying the following relation:

$$\rho_i = \alpha_i\Lambda_i + \beta_i, \ i = 1,2. \tag{11}$$

According to Eqs. (9) and (10), in both regions the area ratio reactivity is based on the local reactivity in the thermal region with a factor and a term describing the coupling effect with

the booster region. One should notice that, in the booster region, the return probability appears in the denominator, thus affecting the result stronger than in the thermal region where the return probability appears in the nominator. The return probability can in this case be interpreted as the influence of the absorbing valve zone. Thus, the more efficient valve zone, the lower is f and the larger is the reactivity deviation in the booster zone. The general trends of Eq. (9) and (10) with respect to f are shown in Fig. 10 and indicates a linear dependence for the thermal region and a strongly non-linear dependence for the booster region. The figure is based on rough estimates of the kinetic parameters for the two regions among Λ_1 is the most crucial one. Assuming a ratio of two between the reactivities and based on a reasonable choice of Λ_1 around 1-2 μs yields a return probability of around 1%. This value should, however, be interpreted with care since higher eigenmodes are not included in this model.

This simple model explains analytically the mechanism behind the strong spatial variation between the fast and the thermal region, but to fully describe the spatial dispersion between all detectors a complete three dimensional continuous energy treatment is needed.

V. SPATIAL CORRECTION FACTORS

In the previous section, a two-region point kinetics model has been presented to explain the deviations observed in the reactivity estimate provided by the Sjöstrand area ratio method in different core regions. Even more, it has been shown that, in general, even among detectors where the dispersion is small, the area method returns a biased estimate of the reactivity. Hence, it is necessary to obtain a correction factor for each detector position which takes into account the complete description of the system. Spatial correction factors for reactivity have been studied previously [18-20], but will here be implemented in an alternative way by embedding, in addition to the spatial effects, also the effective delayed

neutron fraction. It will be shown here that this correction factor can be obtained from MCNP calculations (other simulation tools can also be used to investigate spatial and energy effects for the area method as shown by M. Carta. et al. [20]).

Let us start by rewriting Eq. (1) in the form:

$$\rho_{\$} \equiv \frac{\rho}{\beta_{eff}} = -\frac{A_p}{A_d} = \left(1 - \frac{A_t}{A_p}\right)^{-1}, \tag{12}$$

where A_t denotes the area due to both prompt and delayed neutrons, that is, $A_t = A_p + A_d$. A_t and A_p can be calculated for every detector location with MCNP just enabling or disabling the delayed neutron transport. In this way, MCNP can provide an estimator of the area ratio method dollar reactivity, $\rho_{MCNP,i}$, for any detector position i. On the other hand, a criticality calculation can also be performed with MCNP to obtain a value of the effective multiplication factor, k_{MCNP}, of the system. Thus, a correction factor for the area ratio method in every detector location can be obtained in the following way:

$$C_i = \frac{\rho_{MCNP,i}}{\frac{k_{MCNP}-1}{k_{MCNP}}} = \frac{\rho_{MCNP,i}}{\rho_{MCNP}}, \tag{13}$$

where i represents detector positions EC1B-EC3B, EC5T-EC6T and MC2-MC3. Since $\rho_{MCNP,i}$ is expressed in units of dollars, the correction factor is equal to the reciprocal of the effective delayed neutron fraction if the correction is negligible. Once these correction factors have been obtained, the corrected experimental reactivity value of the system, ρ_{exp}, can be estimated in a straightforward way:

$$\rho_{\exp} = \frac{\rho_{\exp,i}}{\rho_{MCNP,i}} \rho_{MCNP} = \frac{\rho_{\exp,i}}{C_i}, \tag{14}$$

or in the following form giving the corrected experimental k_{eff} directly:

$$k_{eff} = \frac{1}{1 - \frac{\rho_{\exp,i}}{C_i}} \cdot \tag{15}$$

It has been found that this definition of the correction factors has two advantages over the methodology presented in ref. [19], where the effective delayed neutron fraction is not embedded in the correction. Firstly, the correction path is independent of the specific value of the effective delayed neutron fraction, which is consequently not needed to be calculated explicitly and the overall calculation time is reduced. Secondly, in this way a direct estimate of the effective multiplication factor of the system, k_{eff}, can be obtained instead of obtaining an estimate of the reactivity, $\rho_{\$}$, of the system.

The correction factors have been computed using different nuclear data libraries and the reactivity values thus obtained are listed in Table III. It must be pointed out that the observed uncertainty in the determination of the correction factors decreases much slower than the statistical uncertainty in $\rho_{MCNP,i}$, hence, to obtain a good estimate, it is necessary to run each case for the equivalent of 800 processor-days on a state-of-the-art computing cluster.

Inspecting Table III it can be observed that the dispersion of the data is greatly reduced and most of the detector results are compatible among themselves. Furthermore, the reactivity values obtained for the SC3a and SC3b configurations are close, as it was expected according to MCNP simulations.

VI. CONCLUSIONS

A set of pulsed neutron source measurements has been performed in the strongly heterogeneous subcritical assembly YALINA-Booster. It has been found that the area ratio reactivity measurement method of Sjöstrand gives strongly deviating results for detectors located in the fast spectrum part of the core. The deviation was caused by the close location of the detector to the source and the presence of the absorbing valve zone, in addition to the different neutron spectra. The latter two could be explained analytically through a simple two-region point kinetics model and the dispersion could be accounted for by applying correction factors obtained through Monte Carlo calculations.

A new way of obtaining the corrected effective multiplication factor from the measured reactivity in units of dollars, without the need of explicitly calculating the effective delayed neutron fraction, was presented. Thereby, comparable results could be obtained for all detectors and the strong spatial spread was handled.

Further, it was found that the Sjöstrand area ratio method was not affected by a source multiplication perturbation and at deep subcriticality, the method performed equally well as compared to the other configurations. Thus, the same correction procedure could be applied successfully.

A consequence of the local strong deviation of the Sjöstrand area ratio method in a loosely coupled heterogeneous system is that care must be taken when applying this method for calibration purposes in future fast spectrum accelerator-driven systems loaded with high local concentrations of nuclides having large absorption cross section, such as ^{241}Am.

ACKNOWLEDGEMENTS

This work was supported by IP-EUROTRANS contract no. FI6W-CT2005-516520, the ENRESA-CIEMAT agreement for the *Transmutación Aplicada a los Residuos Radiactivos de Alta Actividad*, Svensk Kärnbränslehantering AB (SKB, the Swedish Nuclear Fuel and Waste Management Co) and the Swedish Institute through the *Visby program*.

REFERENCES

1. N. G. SJÖSTRAND, "Measurement on a subcritical reactor using a pulsed neutron source," *Arkiv för fysik* **11**, 13 (1956).
2. R. ROSA, "RACE-T Experimental Activities – A Complete Overview of the Different Subcritical Measurement Techniques," *Proc. of Int. Conf. AccApp'07*, Pocatello, ID, USA, Jul 30 - Aug 2 (2007).
3. C. JAMMES et al., "Absolute Reactivity Calibration of Accelerator-Driven Systems after RACE-T Experiments," *Proc. of PHYSOR 2006*, Vancouver, BC, Canada, Sep. 10-14 (2006).
4. J. JAMMES et al., "Advantage of the area-ratio pulsed neutron source technique for ADS reactivity calibration," *Nuclear Instruments and Methods in Physics Research A* **562**, pp. 778-784 (2006).
5. S. E. CHIGRINOV et al., "Booster Subcritical Assembly Driven by a Neutron Generator," Preprint JIPNR-Sosny, Minsk (2004). (In Russian).

6. J. F LEBRAT et al., “Global Results from Deterministic and Stochastic Analysis of the MUSE-4 Experiments on the Neutronics of Accelerator-Driven Systems,” *Nuclear Science and Engineering* **158**, pp. 49-67 (2008).
7. C. RUBBIA et al., “TRADE: a full experimental validation of the ADS concept in a European perspective,” *Proc. of Int. Conf. AccApp’03*, Jun 1-5, San Diego, California, USA (2003).
8. D. BELLER et al., “Overview of the U.S. reactor-accelerator coupling experiments (RACE) project,” *Proc. of Int. Conf. AccApp’07*, Pocatello, ID, USA, Jul 30 – Aug 2 (2007).
9. C.-M. PERSSON et al., “Analysis of reactivity determination methods in the subcritical experiment Yalina,” *Nuclear Instruments and Methods in Physics Research A* **554**, pp. 374-383 (2005).
10. CANBERRA, www.canberra.com (2009).
11. C. GUERRERO et al., “Analysis of the BC501A neutron detector signals using the true pulse shape,” *Nuclear Instruments and Methods in Physics Research Section A*, **597**, pp. 212-218 (2008).
12. H. KIYAVITSKAYA (coordinator), “YALINA-Booster Benchmark Specifications for the IAEA Coordinated Research Projects on Analytical and Experimental Benchmark Analysis on Accelerator Driven Systems and Low Enriched Uranium Fuel Utilization in Accelerator Driven Sub-Critical Assembly Systems,” IAEA (2007).
13. X-5 MONTE CARLO TEAM, “MCNP – A General Monte Carlo N-Particle Transport Code, Version 5”, LA-UR-03-1987, Los Alamos National Laboratory, USA (2005).
14. M. SAROTTO et al., “Specification for the EFIT core and fuel element,” Deliverable D1.6 of the *European Research Programme for the transmutation of high level nuclear*

waste in an accelerator-driven system within the sixth framework programme, Euratom, Contract no. FI6W-CT-2004-516520 (2008).

15. R. SOULE et al., "Validation of neutronic methods applied to the analysis of fast subcritical systems: The MUSE-2 experiments," *Proc. of Int. Conf. GLOBAL'97*, Yokohama, Japan (1997).
16. D. VILLAMARIN FERNANDEZ, "Análisis dinámico del reactor experimental de fisión nuclear MUSE-4," Doctoral Thesis, Universidad Complutense de Madrid, Departamento de Física Atómica, Molecular y Nuclear, Madrid, Spain (2004).
17. G. D. SPRIGGS et al., "Two-Region Kinetic Model for Reflected Reactors", *Annals of Nuclear Energy*, **24**, No. 3, pp. 205-250 (1997).
18. V. E. KOLESOV et al., DNESTR code and its application for taking into account spatial effects in the course of reactivity measurement by IK method. Preprint FEI-1162, Obninsk, Russia (1981).
19. C. JAMMES, "Modeling of the RACE-ISU subassembly to analyze neutronics experimental data," *Proc. of Int. Conf. AccApp'07*, Pocatello, ID, USA, Jul 30 – Aug 2 (2007).
20. M. CARTA et al. "Reactivity assessment and spatial time-effects from the MUSE kinetics experiments," *Proc. of PHYSOR 2004*, Chicago, Illinois, USA, April 25-29 (2004).
21. THE NUCLEAR ENERGY AGENCY, www.nea.fr (2009).

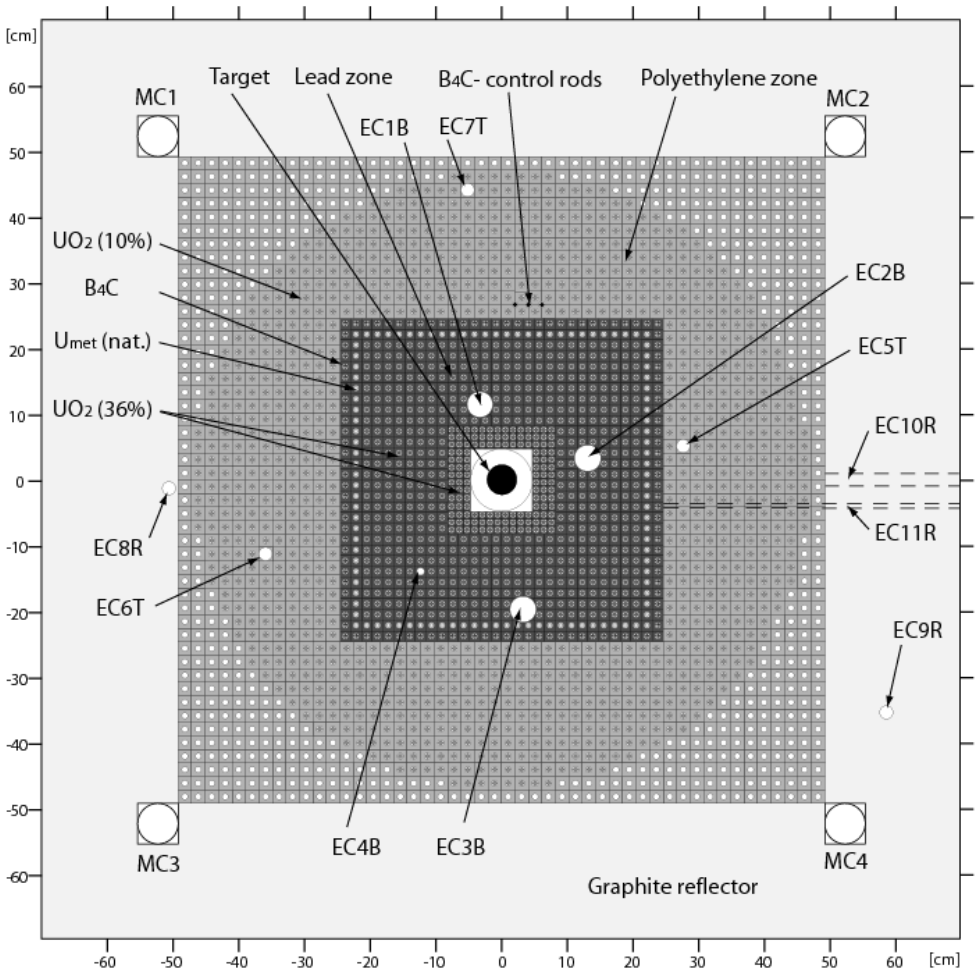

Fig. 1. Schematic cross-sectional view of the YALINA-Booster reactor core (SC3a).

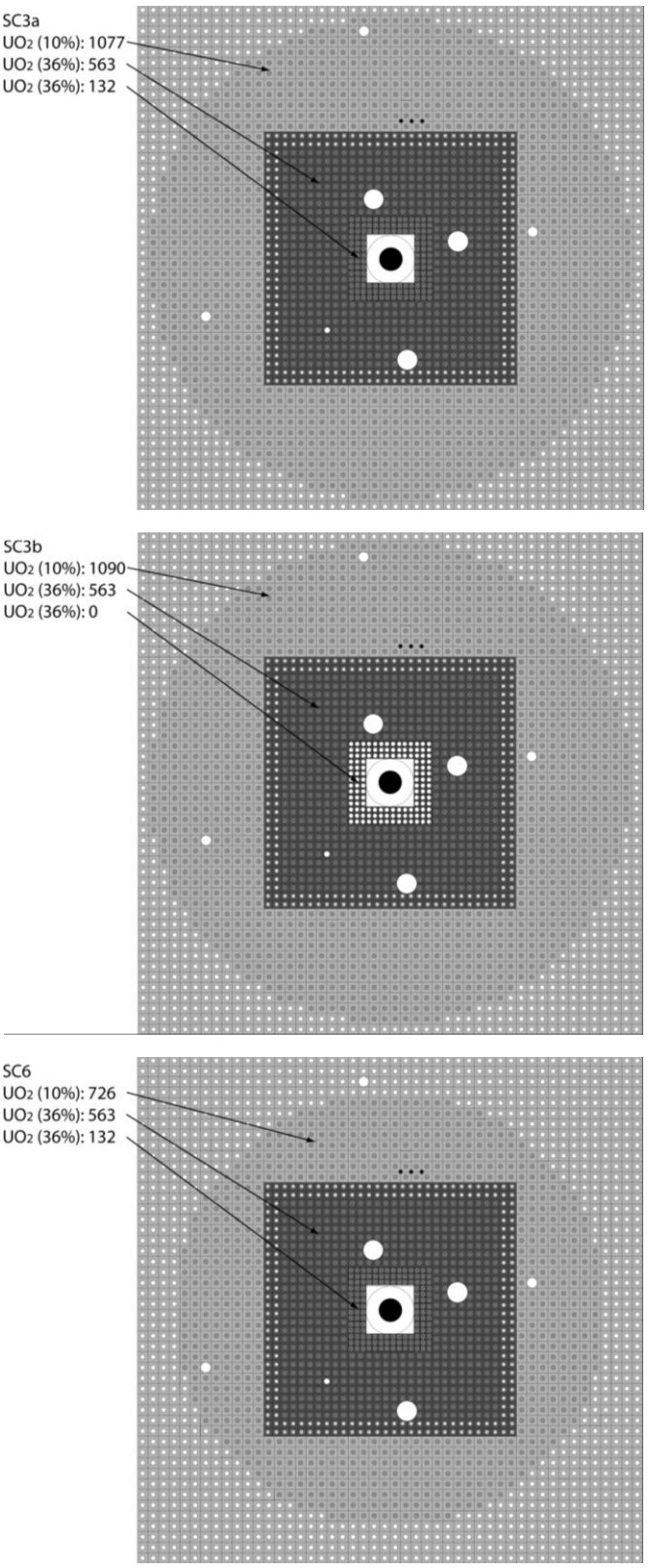

Fig. 2. Core configurations considered for the measurements.

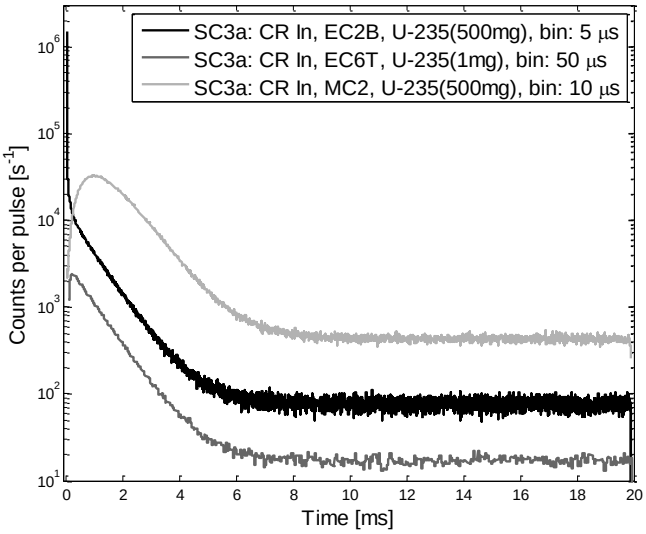

Fig. 3. PNS histograms for configuration SC3a (CR inserted).

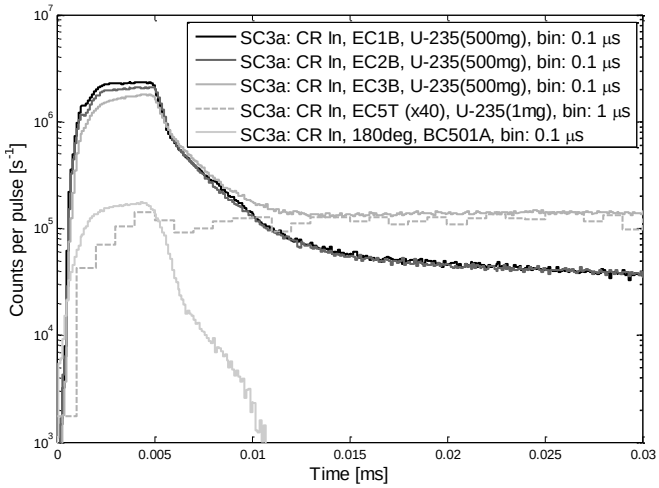

Fig. 4. The first 30 μs of the PNS histograms of the detectors in the booster region, EC5T and the source monitor. The data from EC5T have been multiplied by 40 to better visualize the similarity to EC3B after 15 μs.

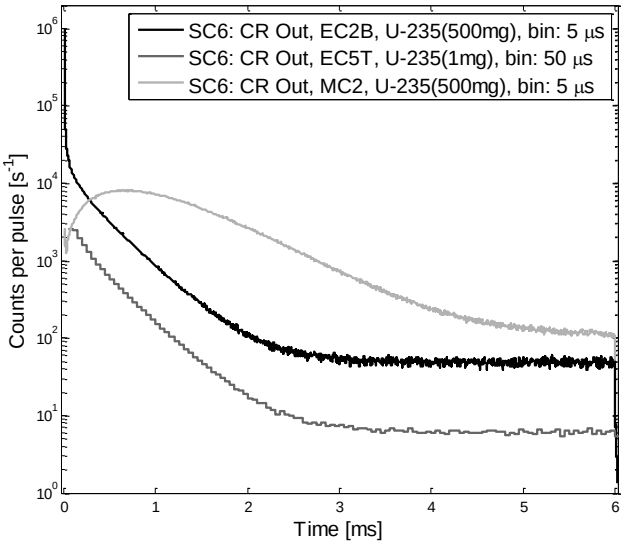

Fig. 5. PNS histograms for configuration SC6.

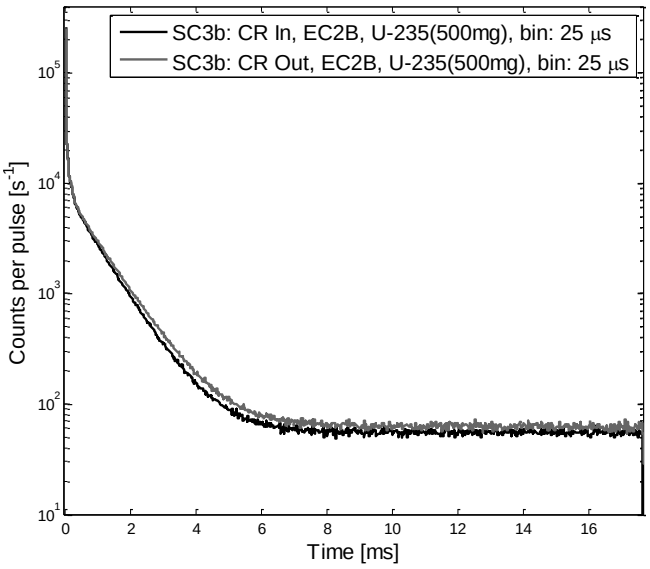

Fig. 6. PNS histograms for configuration SC3b channel EC2B with control rods withdrawn and inserted.

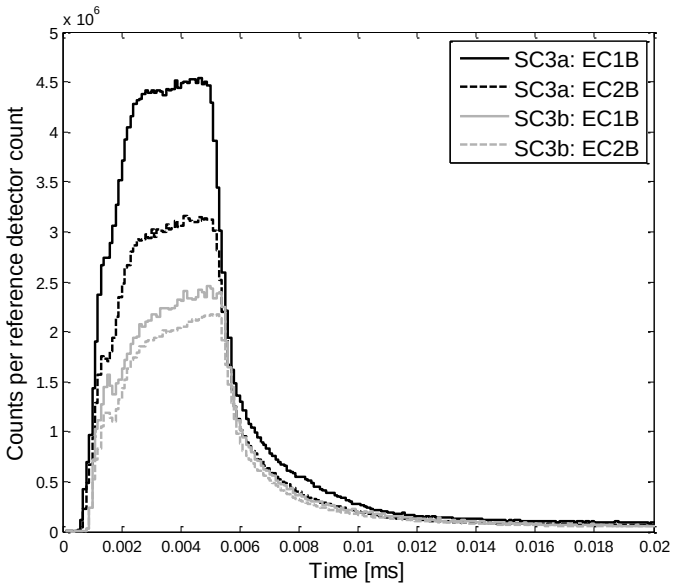

Fig. 7. Zoom of first part of PNS histograms for configurations SC3a and SC3b and detector locations EC1B and EC2B (CR inserted and bin size 0.1 μs).

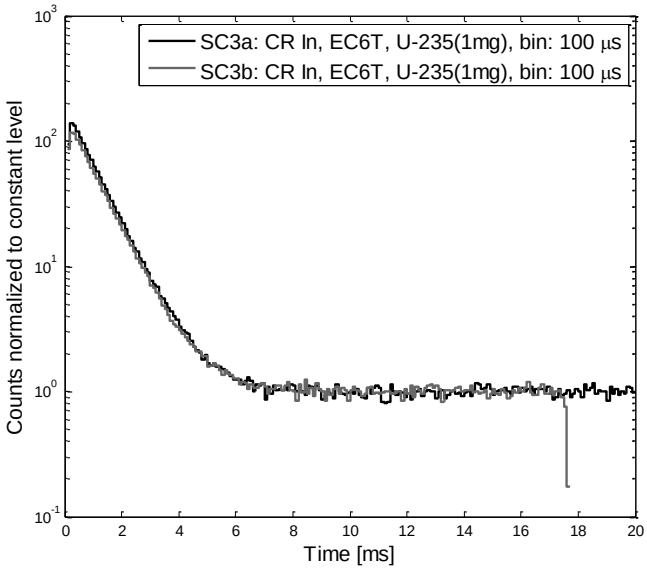

Fig. 8. PNS histograms for SC3a and SC3b at the same detector position. (A shorter period was chosen for SC3b to increase the detector count rates).

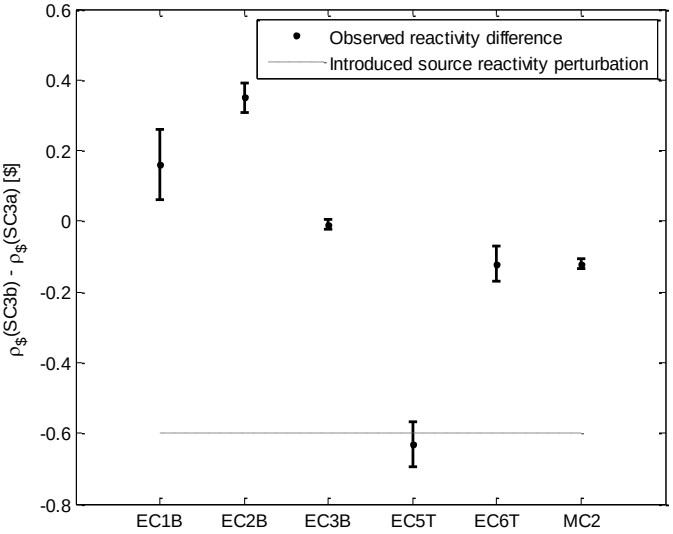

Fig. 9. Reactivity difference between SC3a and SC3b at various detector positions (uncorrected data) and approximate source reactivity perturbation in units of dollars.

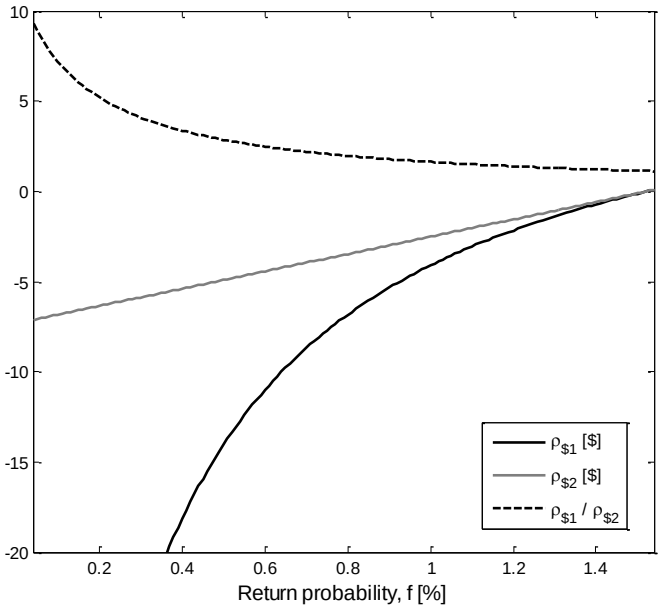

Fig. 10. Area ratio reactivities and their ratio as a function of return probability.

Table I. Core configurations.

	Zone and fuel enrichment			k_{eff}[a]
	Inner booster	Outer booster	Thermal zone	
	36%	36%	10%	
SC3a	132	563	1077	0.950
SC3b	0	563	1090	0.950
SC6	132	563	726	0.850

[a] Expected value based on Monte Carlo [13] simulations.

Table II. Experimental results without corrections.

		$\rho_{\$}$ [$]	
		CR Out	CR In
SC3a	EC1B	-15.31±0.03	-17.64±0.04
	EC2B	-	-15.63±0.03
	EC3B	-	-10.20±0.01
	EC5T	-8.70±0.06	-9.44±0.04
	EC6T	-	-7.48±0.03
	MC2	-7.23±0.01	-7.85±0.01
	MC3	-7.24±0.18	-7.88±0.21
SC3b	EC1B	-15.17±0.07	-17.48±0.09
	EC2B	-13.92±0.02	-15.28±0.03
	EC3B	-9.64±0.01	-10.21±0.01
	EC5T	-9.26±0.04	-10.07±0.05
	EC6T	-7.42±0.04	-7.60±0.04
	MC2	-7.31±0.01	-7.97±0.01
SC6	EC2B	-43.63±0.07	-
	EC5T	-23.96±0.85	-
	MC2	-20.12±0.18	-

Table III. Correction factors obtained from the evaluated nuclear data libraries ENDF/B-VII, JEFF3.1 and JENDL-3.3 [21] and corrected values of the effective multiplication factor.

SC3a CR Out	C_i			k_{eff}		
	ENDF/B-VII	JEFF-3.1	JENDL-3.3	ENDF/B-VII	JEFF-3.1	JENDL-3.3
EC1B	269.58 ± 2.19	265.81 ± 1.64	273.45 ± 2.23	0.94626 ± 0.00045	0.94554 ± 0.00035	0.94698 ± 0.00044
EC2B	244.70 ± 1.83	238.40 ± 1.33	246.13 ± 1.84	---	---	---
EC3B	166.73 ± 1.55	161.29 ± 1.25	164.46 ± 1.50	---	---	---
EC5T	150.26 ± 1.95	143.63 ± 1.51	148.18 ± 1.89	0.94527 ± 0.00080	0.94289 ± 0.00072	0.94454 ± 0.00080
EC6T	129.41 ± 1.48	124.67 ± 1.06	126.10 ± 1.40	---	---	---
MC2	125.26 ± 1.39	125.09 ± 1.07	125.01 ± 1.36	0.94543 ± 0.00061	0.94536 ± 0.00047	0.94533 ± 0.00061
MC3	126.30 ± 1.41	122.43 ± 1.12	124.02 ± 1.38	0.94578 ± 0.00148	0.94416 ± 0.00148	0.94484 ± 0.00150
Weighted average				0.94585 ± 0.00025	0.94510 ± 0.00051	0.94604 ± 0.00058

SC3a CR In	C_i			k_{eff}		
	ENDF/B-VII	JEFF-3.1	JENDL-3.3	ENDF/B-VII	JEFF-3.1	JENDL-3.3
EC1B	292.83 ± 2.67	287.56 ± 2.10	294.34 ± 2.19	0.94318 ± 0.00053	0.94220 ± 0.00044	0.94346 ± 0.00044
EC2B	252.94 ± 2.03	248.28 ± 1.60	255.78 ± 1.69	0.94180 ± 0.00048	0.94078 ± 0.00040	0.94241 ± 0.00040
EC3B	165.11 ± 1.59	159.60 ± 1.34	163.27 ± 1.23	0.94182 ± 0.00056	0.93993 ± 0.00051	0.94120 ± 0.00045
EC5T	152.91 ± 2.11	146.55 ± 1.68	151.08 ± 1.78	0.94185 ± 0.00084	0.93948 ± 0.00074	0.94119 ± 0.00074
EC6T	128.86 ± 1.54	122.45 ± 1.20	125.48 ± 1.26	0.94514 ± 0.00069	0.94243 ± 0.00061	0.94374 ± 0.00061
MC2	129.60 ± 1.55	127.00 ± 1.29	127.81 ± 1.30	0.94289 ± 0.00069	0.94179 ± 0.00059	0.94214 ± 0.00059
MC3	125.71 ± 1.57	121.64 ± 1.19	121.77 ± 1.19	0.94102 ± 0.00174	0.93916 ± 0.00173	0.93922 ± 0.00173
Weighted average				0.94263 ± 0.00046	0.94114 ± 0.00042	0.94236 ± 0.00041

SC3b CR Out	C_i			k_{eff}		
	ENDF/B-VII	JEFF-3.1	JENDL-3.3	ENDF/B-VII	JEFF-3.1	JENDL-3.3
EC1B	286.89 ± 3.39	286.83 ± 3.35	297.39 ± 3.11	0.94978 ± 0.00064	0.94977 ± 0.00063	0.95147 ± 0.00055
EC2B	259.96 ± 2.43	254.83 ± 2.32	268.69 ± 2.57	0.94918 ± 0.00048	0.94820 ± 0.00048	0.95074 ± 0.00048
EC3B	168.81 ± 1.42	165.42 ± 1.36	170.45 ± 1.44	0.94598 ± 0.00046	0.94493 ± 0.00046	0.94647 ± 0.00046
EC5T	151.53 ± 1.85	147.80 ± 1.75	150.62 ± 1.82	0.94241 ± 0.00075	0.94104 ± 0.00074	0.94208 ± 0.00074
EC6T	128.17 ± 1.26	125.63 ± 1.20	129.73 ± 1.28	0.94528 ± 0.00061	0.94423 ± 0.00061	0.94590 ± 0.00061
MC2	128.38 ± 1.26	125.81 ± 1.20	127.43 ± 1.24	0.94613 ± 0.00053	0.94509 ± 0.00053	0.94575 ± 0.00053
MC3	128.40 ± 1.36	126.71 ± 1.32	127.35 ± 1.33	---	---	---
Weighted average				0.94677 ± 0.00097	0.94585 ± 0.00110	0.94759 ± 0.00130

SC3b CR In	C_i			k_{eff}		
	ENDF/B-VII	JEFF-3.1	JENDL-3.3	ENDF/B-VII	JEFF-3.1	JENDL-3.3
EC1B	314.09 ± 4.80	305.33 ± 4.57	319.99 ± 4.37	0.94728 ± 0.00085	0.94585 ± 0.00086	0.94820 ± 0.00076
EC2B	273.38 ± 2.79	266.17 ± 2.67	279.53 ± 2.91	0.94707 ± 0.00055	0.94571 ± 0.00055	0.94817 ± 0.00055
EC3B	168.86 ± 1.48	164.04 ± 1.42	168.53 ± 1.48	0.94298 ± 0.00050	0.94141 ± 0.00051	0.94288 ± 0.00050
EC5T	155.35 ± 2.02	148.05 ± 1.86	152.36 ± 1.95	0.93913 ± 0.00085	0.93632 ± 0.00086	0.93800 ± 0.00085
EC6T	129.14 ± 1.33	125.12 ± 1.26	127.78 ± 1.30	0.94442 ± 0.00064	0.94273 ± 0.00065	0.94386 ± 0.00064
MC2	131.96 ± 1.38	128.08 ± 1.32	130.32 ± 1.35	0.94304 ± 0.00060	0.94142 ± 0.00061	0.94237 ± 0.00060
MC3	128.61 ± 1.42	124.59 ± 1.35	126.38 ± 1.38	---	---	---
Weighted average				0.94415 ± 0.00106	0.94250 ± 0.00121	0.94423 ± 0.00138

SC6 CR Out	C_i			k_{eff}		
	ENDF/B-VII	JEFF-3.1	JENDL-3.3	ENDF/B-VII	JEFF-3.1	JENDL-3.3
EC1B	304.96 ± 6.66	288.35 ± 9.63	296.73 ± 6.25	---	---	---
EC2B	268.15 ± 7.74	258.62 ± 7.17	262.55 ± 7.36	0.86006 ± 0.00404	0.85565 ± 0.00401	0.85750 ± 0.00400
EC3B	164.20 ± 4.90	161.81 ± 4.74	157.76 ± 4.49	----	----	---
EC5T	138.88 ± 6.34	136.30 ± 6.09	136.18 ± 5.72	0.85287 ± 0.00674	0.85049 ± 0.00670	0.85038 ± 0.00631
EC6T	115.40 ± 4.42	108.05 ± 3.87	110.67 ± 4.04	---	---	---
MC2	124.78 ± 6.86	115.01 ± 5.82	112.38 ± 5.54	0.86115 ± 0.00666	0.85111 ± 0.00651	0.84815 ± 0.00645
MC3	118.74 ± 6.74	120.76 ± 6.94	114.70 ± 6.25	---	---	---
Weighted average				0.85880 ± 0.00217	0.85359 ± 0.00170	0.85389 ± 0.00293